PSFC/JA-11-8

Forces on a spherical conducting particle in ExB fields

L. Patacchini
I. H. Hutchinson

May 2011

Plasma Science and Fusion Center
Massachusetts Institute of Technology
Cambridge MA 02139 USA

Submitted for publication to *Plasma Physics and Controlled Fusion*.

This work was supported in part by the U.S. Department of Energy, Grant No. DE-FG02-06ER54891.

Forces on a spherical conducting particle in $\mathbf{E} \times \mathbf{B}$ fields

Leonardo Patacchini and Ian H. Hutchinson

Plasma Science and Fusion Center, MIT

Abstract

The forces acting on a spherical conducting particle in a transversely flowing magnetized plasma are calculated in the entire range of magnetization and Debye length, using the particle code SCEPTIC3D [Patacchini and Hutchinson, Plasma Phys. Control. Fusion **52** 035005 (2010), Plasma Phys. Control. Fusion **53** 025005 (2011)]. In short Debye length (i.e. high density) plasmas, both the ion-drag and Lorentz force arising from currents circulating inside the dust show strong components antiparallel to the convective electric field, suggesting that a free dust particle should gyrate faster than what predicted by its Larmor frequency. In intermediate to large Debye length conditions, by a downstream depletion effect already reported in unmagnetized strongly collisional regimes, the ion-drag in the direction of transverse flow can become negative. The internal Lorentz force however remains in the flow direction, and large enough in magnitude so that no spontaneous dust motion should occur.

1 Introduction

The computation of forces acting on a spherical particle in a uniform, collisionless flowing plasma is an idealized problem of key importance to the understanding of dust dynamics [1]. Fully analytic treatments are typically limited to the unmagnetized, large Debye length regime where the ion trajectories have simple expressions. Numerical simulations are otherwise necessary, and the first comprehensive investigation of the unmagnetized regime was performed with the 2D3v Particle In Cell (PIC) code SCEPTIC [2, 3]. The purpose of this publication is to extend the analysis to magnetized conditions where the background plasma has an "$\mathbf{E} \times \mathbf{B}$"-driven transverse flow (or equivalently the collecting sphere or "dust" drifts across the magnetic field lines), using the 3D3v code version SCEPTIC3D [4, 5].

In the absence of external fields and ion-neutral interactions, force calculations based on the binary collision approach are perhaps the most intuitive. Momentum conservation requires that, in steady state, the force felt by the dust be equal to the rate of momentum flux through any surrounding control surface. By taking such a surface at "infinity", where the plasma potential is unperturbed, the force naturally splits in an "ion impact" term $\mathbf{F}^{\infty}_{\mathbf{im}}$ and an "orbital" term $\mathbf{F}^{\infty}_{\mathbf{E}}$, respectively arising from collected and deflected ions. Their sum $\mathbf{F_i} = \mathbf{F}^{\infty}_{\mathbf{im}} + \mathbf{F}^{\infty}_{\mathbf{E}}$ is usually referred to as the ion-drag force. When the plasma shielding length Λ_s is much larger than the dust dimensions, there are no intermediate effective potential barriers and each ion whose energy and angular momentum at infinity is compatible with collection is collected. In this Orbit Motion Limited (OML) regime [6], the ion impact force $\mathbf{F}^{\infty}_{\mathbf{im}}$ can be computed analytically, and calculation of $\mathbf{F}^{\infty}_{\mathbf{E}}$ reduces to the usual Coulomb collision problem [2, 7]. When Λ_s is not large enough for the OML assumption to be valid, the binary-collision approach can still be used although analytic

calculations are typically not possible. For instance, direct orbit integration (i.e. non self-consistent) simulations have been performed by Khrapak and coauthors [8] with the assumption of a Debye-Hückel potential distribution.

The binary-collision approach is however difficult to use in situations where the momentum of the "dust + ions" system is not conserved, because it is then necessary to compute their momentum loss while orbiting before collection. Forces are then most easily computed as physically felt by the particle at its surface. This happens in the presence of external electric and magnetic fields, the focus of this work, but also for instance in the presence of ion-neutral collisions. In unmagnetized systems: $\mathbf{F_i} = \mathbf{F^p_{im}} + \mathbf{F^p_E} + \mathbf{F^p_e}$, where $\mathbf{F^p_{im}}$ corresponds to the ion impact term at the surface ($\neq \mathbf{F^\infty_{im}}$ because ions are accelerated before collection), $\mathbf{F^p_E}$ ($\neq \mathbf{F^\infty_E}$) corresponds to the electrostatic stress at the surface, and $\mathbf{F^p_e}$ is the typically negligible electron pressure on a negatively biased collector. In the so-called point-like dust approximation, when Λ_s is much larger than the thermal 90^0 scattering impact-parameter, $\mathbf{F^p_{im}}$ is negligible compared to $\mathbf{F^p_E}$. Calculations using the dielectric response formalism, whose gist is to calculate the anisotropic part of the potential distribution from the plasma permittivity and apply it to the dust charge, can then be performed. Analytic solutions have been given in the limit of weak [9] and srong [10] collisionality.

Similar linearized calculations in cross-flowing magnetized plasmas might be possible, but a closed-form expression for the potential distribution is unlikely if the full hot magnetoplasma susceptibility tensor is to be used. Calculations are nevertheless tractable when using the cold plasma equations, in particular in the absence of convective electric field (only parallel flow) [11]; they show that the potential distribution around the test charge decays to zero at infinity only when the flow Mach number is higher than unity. This is an alternative way to understand the fact that no self-consistent solution to the *collisionless* plasma-probe interaction problem in parallel-flowing magnetoplasmas exists unless $\Lambda_s = \infty$ *exactly* (ions and electrons are then decoupled), or the magnetized Bohm condition (parallel Mach number larger than unity) is pre-satisfied in the unperturbed plasma [12]. In this publication, we limit ourselves to situations where the cross-field drift is non-zero.

Because SCEPTIC3D models the plasma dynamics self-consistently with the electrostatic potential distribution, it can compute the ion-drag force at the outer boundary of its computational domain (loosely corresponding to a binary collision view), or at the dust surface. In addition to the ion-drag, it is important to account for the action of the convective field on the dust charge $\mathbf{F^p_Q}$, and for the Lorentz force arising from currents circulating inside the dust $\mathbf{F^p_j}$. Of course in experimental configurations other effects such as neutral drag, thermophoretic force, rocket ablation force, radiation pressure, and so on, might be significant but we shall not here discuss them further.

The computational method for force calculations is described in section 2. We then proceed with benchmarks against free-flight calculations and momentum conservation requirements (section 3), and with the presentation and discussion of our self-consistent results (section 4).

2 Method for force calculations

2.1 SCEPTIC3D

SCEPTIC3D is a 3D3v hybrid electrostatic PIC code [13, 14], introduced in Refs [4, 5] to study ion collection by negatively charged spheres (in practice probes or dust particles) in "$\mathbf{E} \times \mathbf{B}$" fields.

A spherical conducting dust particle of radius R_p is located at the origin of a uniform plasma with ion and electron charge-densities $ZN_i = N_e = N_\infty$, temperatures $T_{i\infty}$ and T_e, and electron Debye length $\Lambda_{De} = \left(\epsilon_0 T_e / e^2 N_\infty\right)^{1/2}$. The model consists of Lagrangian ions whose coordinates $\mathbf{x} = (x, y, z)^T$ are governed by Newton's equation

$$\frac{m}{Ze}\frac{\mathrm{d}^2\mathbf{x}}{\mathrm{d}t^2} = \mathbf{E} + \frac{\mathrm{d}\mathbf{x}}{\mathrm{d}t} \times \mathbf{B}, \tag{1}$$

and isothermal electrons with Boltzmann density

$$N_e = N_\infty \exp\left(\frac{e\Phi}{T_e}\right). \tag{2}$$

The ion orbit integration is performed with the method of Ref. [15]. A uniform external magnetic field $\mathbf{B}$ and a uniform convective electric field $\mathbf{E}_{\mathrm{conv}}$ drive a background cross-field drift $\mathbf{v}_\perp = \mathbf{E}_{\mathrm{conv}} \times \mathbf{B}/\mathbf{B}^2$; hence in Eqs (1,2) Φ is the dust-induced potential perturbation, and $\mathbf{E} = \mathbf{E}_{\mathrm{conv}} - \nabla\Phi$ is the total electric field acting on the ions and electrons. The total drift velocity is $\mathbf{v_d} = \mathbf{v}_\perp + \mathbf{v}_\infty$, where the parallel external drift, $\mathbf{v}_\infty$, can be chosen freely.

Integration of the perpendicular electron momentum equation shows that in this "Boltzmann" regime, the electron cross-field fluid velocity is everywhere equal to the *background* "$\mathbf{E}\times\mathbf{B}$" velocity regardless of Φ, because diamagnetic drift exactly cancells the additional "$\nabla\phi \times \mathbf{B}$" drift:

$$\langle \mathbf{v_e} \rangle_\perp = \mathbf{E}_{\mathrm{conv}} \times \frac{\mathbf{B}}{\mathbf{B}^2}, \tag{3}$$

while the ion cross-field velocity is perturbed in the dust neighborhood and must be self-consistently resolved by the code.

The computational domain has a spherical geometry in order to accurately resolve the plasma-surface boundary, as illustrated in Fig. (1). R is the radial distance measured from the dust center, $\theta \in [0 : \pi]$ is the polar angle measured from the magnetic axis ($\mathbf{e_z}$), and $\psi \in [0 : 2\pi]$ is the azimuthal angle measured from the plane of convective and magnetic fields (the $\{\mathbf{e_x}, \mathbf{e_z}\}$-plane). The angle between $\mathbf{B}$ and $\mathbf{v_d}$ is denoted δ, and ρ is the cylindrical radius from the magnetic axis.

The code uses non-dimensional quantities. The potential ϕ is in units of T_e/e ($\phi = e\Phi/T_e$), distances in dust radii R_p, and charge-densities in N_∞. Dimensionless distances and densities are indicated by lower-case characters ($\lambda_{De} = \Lambda_{De}/R_p$, $n_i = ZN_i/N_\infty$, etc.). The magnetic field strength is defined as the ratio of the dust radius to the mean ion Larmor radius at infinity

$$\beta_i = \frac{R_p}{R_L} = ZeBR_p \left(\frac{2}{\pi m T_{i\infty}}\right)^{1/2}. \tag{4}$$

For convenience we also define the thermal energy ratio $\tau = T_{i\infty}/ZT_e$, velocities normalized by the ion thermal speed $w = v/v_{ti}$ ($v_{ti} = (2T_{i\infty}/m)^{1/2}$), and the potential in ion thermal units $\chi = -Ze\Phi/T_{i\infty}$.

In Refs [4, 5] charge flux-densities were scaled to the random thermal charge flux-density $\Gamma^0_{i,e} = N_\infty v_{ti,e}/\left(2\sqrt{\pi}\right)$, and currents to $I^0_{i,e} = 4\pi R_p^2 \Gamma^0_{i,e}$. Here forces will be scaled to the unperturbed ion or electron pressure forces over a sample surface R_p^2:

$$F^0_i = N_\infty R_p^2 T_{i\infty}/Z, \tag{5}$$

$$F^0_e = N_\infty R_p^2 T_e. \tag{6}$$

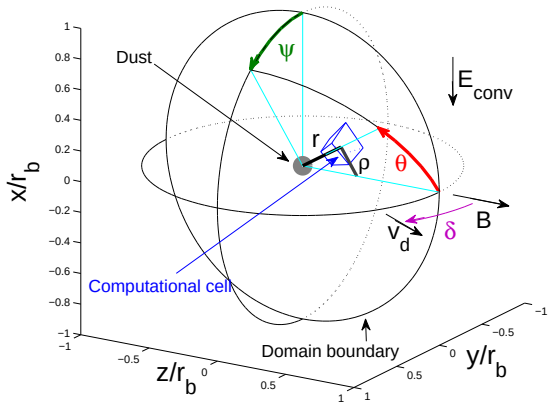

Figure 1: Three-dimensional view of the computational domain in spherical coordinates (modified from [4]).

ϕ is the solution of the dimensionless Poisson-Boltzmann equation $\nabla^2\phi = (\exp\phi - n_i)/\lambda_{De}^2$, with "conducting" inner boundary condition

$$\phi(R_p, \theta, \psi) = \phi_p + \phi_{\rm conv} \sin\theta \cos\psi. \tag{7}$$

The median dust potential ϕ_p is referred to as the "dust potential" for simplicity, and

$$\phi_{\rm conv} = \frac{e}{T_e}\left[E_{\rm conv} R_p\right] \tag{8}$$

is a dimensionless measure of the potential variation in the $\mathbf{e_x}$ direction ($\phi_{\rm conv} \leq 0$). At the outer boundary of the computational domain we employ a quite complex condition whose practical effect is to ensure quasineutrality ($n_i = n_e = \exp\phi$); the potential there (as well as its gradient) will therefore be small, but non zero. The ions are reinjected at the outer boundary according to a shifted Maxwellian distribution function. (See Ref. [5] for more details on the boundary conditions and the Poisson solver.)

2.2 Inventory of forces

The total force felt by a (dust) particle is equal to the flux of momentum to its surface, which in a magnetized plasma splits into

- an ion impact force $\mathbf{F_{im}^p}$, equal to the rate of momentum transfer from collected ions,
- the electron pressure integrated over the particle surface $\mathbf{F_e^p}$, which is negligible within our strongly electron-repelling assumption, and

- electrostatic and magnetostatic stresses

$$\tilde{\mathbf{F}}^{\mathbf{p}}_{\mathbf{E}} = \int_S \bar{\bar{\sigma}}_E \cdot \mathrm{d}\mathbf{S} = \mathbf{F}^{\mathbf{p}}_{\mathbf{Q}} + \mathbf{F}^{\mathbf{p}}_{\mathbf{E}}, \tag{9}$$

$$\tilde{\mathbf{F}}^{\mathbf{p}}_{\mathbf{B}} = \int_S \bar{\bar{\sigma}}_B \cdot \mathrm{d}\mathbf{S} = \mathbf{F}^{\mathbf{p}}_{\mathbf{j}}, \tag{10}$$

where

$$\bar{\bar{\sigma}}_E = \epsilon_0 \left(\mathbf{EE} - \frac{1}{2} E^2 \bar{\bar{I}} \right) \quad \text{and} \quad \bar{\bar{\sigma}}_B = \frac{1}{\mu_0} \left(\mathbf{BB} - \frac{1}{2} B^2 \bar{\bar{I}} \right) \tag{11}$$

are the electrostatic and magnetostatic Maxwell stress tensors.

In Eq. (9), $\bar{\bar{\sigma}}_E$ was expanded with $\mathbf{E} = \mathbf{E}_{\mathrm{conv}} - \nabla\Phi$ to show that $\tilde{\mathbf{F}}^{\mathbf{p}}_{\mathbf{E}}$ is sum of

$$\mathbf{F}^{\mathbf{p}}_{\mathbf{Q}} = -\epsilon_0 \int_S \nabla_r \Phi \cdot \mathrm{d}\mathbf{S}\ \mathbf{E}_{\mathrm{conv}} = Q\mathbf{E}_{\mathrm{conv}}, \tag{12}$$

the external electrostatic force acting on the total dust charge Q, and

$$\mathbf{F}^{\mathbf{p}}_{\mathbf{E}} = \epsilon_0 \int_S \left(\nabla\Phi\nabla\Phi - \frac{1}{2} (\nabla\Phi)^2 \bar{\bar{I}} \right) \cdot \mathrm{d}\mathbf{S}, \tag{13}$$

effect of the flow-induced potential distribution anisotropy on the particle.

The SCEPTIC3D code is purely electrostatic and the plasma dynamics is governed by the background magnetic field $\mathbf{B}$ only. The ions, the plasma electrons as well as the electrons moving *in* the conducting particle nevertheless carry currents, inducing a first order correction to $\mathbf{B}$ such that $\mathbf{B} \to B\mathbf{e_z} + \delta\mathbf{B}$ with $\delta B \ll B$. It is then straightforward to show that the magnetic stress on the particle surface reduces to the usual Lorentz force integrated over its volume

$$\mathbf{F}^{\mathbf{p}}_{\mathbf{j}} = \left(\int_\Omega \mathbf{j} \mathrm{d}\Omega \right) \times \mathbf{B}, \tag{14}$$

where $\mathbf{j} = \nabla \times \delta\mathbf{B}/\mu_0$ is the net internal current density.

We refer in this publication to the "ion-drag force" as the fraction of force which can directly be traced back to the plasma flow, and to the "external force" as the action on the particle of the external $\mathbf{E}_{\mathrm{conv}}$ and $\mathbf{B}$ fields. $\mathbf{F}^{\mathbf{p}}_{\mathbf{im}}$, $\mathbf{F}^{\mathbf{p}}_{\mathbf{E}}$ and the negligible $\mathbf{F}^{\mathbf{p}}_{\mathbf{e}}$ are therefore ion-drag force components, and $\mathbf{F}^{\mathbf{p}}_{\mathbf{Q}}$ and $\mathbf{F}^{\mathbf{p}}_{\mathbf{j}}$ external force components. The superscripts "$\mathbf{p}$" here remind us that the contributions are to be evaluated at the particle surface. $\mathbf{F}^{\mathbf{p}}_{\mathbf{im}}$ is calculated by averaging the collected ion momentum rate over the last 25% of the simulation time-steps, while $\mathbf{F}^{\mathbf{p}}_{\mathbf{Q}}$ and $\mathbf{F}^{\mathbf{p}}_{\mathbf{E}}$ are evaluated by differentiation of the potential distribution on each computational cell center located at the dust surface ($r = 1$).

Calculation of $\mathbf{F}^{\mathbf{p}}_{\mathbf{j}}$ is not as straightforward. Indeed while ion codes such as SCEPTIC3D are much faster than their counterpart with full resolution of the electron motion, they do not compute the electron current. Therefore because the net current density $\mathbf{j}$ in the dust particle is solution of the conservation equation $\nabla \cdot \mathbf{j} = 0$ with boundary conditions set by the ion and electron flux-densities to the surface $\Gamma_{i,e}\,(r = 1, \theta, \psi)$, it is impossible to solve Eq. (14) exactly; a reasonable approximate treatment is proposed in section 2.3. Furthermore, we cannot solve the plasma-dust interaction with a self-consistent floating potential balancing ion and electron collection, rather we need to consider the sphere median potential Φ_p as an input, as in [5].

2.3 Internal Lorentz force

2.3.1 Electron current to the dust

The *unmagnetized* electron flux density to the dust particle is equal to the free-space one-dimensional flux density scaled down by the same factor as N_e:

$$\Gamma_e^{B=0} = \Gamma_e^0 \exp \phi_p, \tag{15}$$

giving for the total current to an equipotential repelling sphere of radius R_p:

$$I_e^{B=0} = I_e^0 \exp \phi_p, \tag{16}$$

where we recall $\Gamma_e^0 = N_\infty v_{te}/2\sqrt{\pi}$ and $I_e^0 = 4\pi R_p^2 \Gamma_e^0$.

The derivation of Eq. (15) assumes that (a) the electron drift velocity is much smaller than $v_{te} = (2T_e/m_e)^{1/2}$, which is always true in our Boltzmann (i.e. massless) electron treatment, and (b) that all the orbits striking the sphere are connected to infinity, which is again true if $B = 0$. When a background magnetic field is present however, (b) is no longer a good approximation. The flux is reduced because some helical orbits intersect the sphere several times. Orbit arcs that intersect the sphere at both ends are unpopulated.

In the opposite limit of *infinitesimal Larmor radius*, the electrons move one-dimensionally along the field, and encounter only the projection of the dust area in the field direction. Even if the typical plasma velocities are much smaller than v_{te}, a cross-field drift originating from a convective electric field $\mathbf{E}_{\rm conv}$ strongly affects electron collection because the dust potential in that case is not uniform, rather given by Eq. (7). Therefore the current for $B = \infty$ can be written:

$$\begin{aligned} I_e^{B=\infty} &= 2R_p^2 N_\infty \frac{v_{te}}{2\sqrt{\pi}} \int_{\rho=0}^{1} \int_{\psi=0}^{2\pi} \exp\left(\phi_p + \phi_{\rm conv}\rho\cos\psi\right) \rho \mathrm{d}\rho \mathrm{d}\psi \\ &= I_e^0 \exp\left(\phi_p\right) \frac{\mathtt{I}_1\left(\phi_{\rm conv}\right)}{\phi_{\rm conv}}. \end{aligned} \tag{17}$$

where $\mathtt{I}_n$ is the modified Bessel function defined by

$$\mathtt{I}_n(x) = \frac{1}{\pi} \int_0^\pi \exp(x\cos\alpha)\cos(n\alpha)\mathrm{d}\alpha. \tag{18}$$

If $|\phi_{\rm conv}| \ll 1$ (i.e. $|E_{\rm conv} R_p| \ll T_e/e$), the strongly magnetized electron current given by Eq. (17) is half the unmagnetized one (Eq. (16)). For a discussion of how to bridge the gap between the limits $B = 0$ and $B = \infty$ in the absence of cross-field drift, the reader is referred to Ref. [16]. In this publication, an accurate computation of the electron current will not be attempted.

2.3.2 Internal Lorentz force

Solving the conservation equation $\nabla \cdot \mathbf{j} = 0$ in the dust would yield the full inner 3D current distribution, which is more information than we need. We require only the moments of the current that give rise to the total transverse magnetic force whose components can be obtained by integration by parts directly in terms of the surface current:

$$F^p_{j,y} = eB \int_S x \left(\Gamma_i - \Gamma_e\right) \mathrm{d}S, \tag{19}$$

$$F^p_{j,x} = -eB \int_S y \left(\Gamma_i - \Gamma_e\right) \mathrm{d}S. \tag{20}$$

We now face the same problem as in calculating the electron current (section 2.3.1), i.e. SCEPTIC3D does not calculate Γ_e. Under the reasonable assumption that the repelled electron flux-density only depends on the local dust potential (function of x) and the angle of magnetic field to dust normal (function of z), the first $\mathbf{e_y}$-moment of the electron flux-density is null hence the force in the $\mathbf{e_x}$ direction is governed by ion collection only

$$F^p_{j,x} = -eB \int_S y \Gamma_i \mathrm{d}S. \tag{21}$$

Unfortunately, no such symmetry principle gives $F^p_{j,y}$. In the limit of strongly magnetized electrons however, they only see the projection of the sphere along the magnetic field lines, and we can write (using $x = \rho \cos\psi$):

$$F^p_{j,y} = eB \left[\int_S x \Gamma_i \mathrm{d}S - 2R_p^3 N_\infty \frac{v_{te}}{2\sqrt{\pi}} \int_{\rho=0}^{1} \int_{\psi=0}^{2\pi} \exp\left(\phi_p + \phi_{\mathrm{conv}} \rho \cos\psi\right) \rho^2 \cos\psi \mathrm{d}\rho \mathrm{d}\psi \right]. \tag{22}$$

After integration,

$$F^p_{j,y} = eB \left[\int_S x \Gamma_i \mathrm{d}S - I_e^0 R_p \frac{\exp\phi_p}{\phi_{\mathrm{conv}}} \left(\mathtt{I}_0\left(\phi_{\mathrm{conv}}\right) - 2\frac{\mathtt{I}_1\left(\phi_{\mathrm{conv}}\right)}{\phi_{\mathrm{conv}}} \right) \right]. \tag{23}$$

Although rigorously valid only for infinitesimal electron larmor radius, this expression also has correct $B \to 0$ ($\phi_{\mathrm{conv}} \to 0$) limit. Using Eq. (17), and setting the electron and ion total currents equal for a floating sphere, the force can be written

$$F^p_{j,y} = eB \left[\int_S x \Gamma_i \mathrm{d}S - I_i R_p \left(\frac{\mathtt{I}_0\left(\phi_{\mathrm{conv}}\right)}{\mathtt{I}_1\left(\phi_{\mathrm{conv}}\right)} - \frac{2}{\phi_{\mathrm{conv}}} \right) \right]. \tag{24}$$

This is then a very robust approximation that requires knowledge only of the ion current. Actually here SCEPTIC3D is run with fixed potential (rather than floating) and most of the uncertainties come from possible differences between these[1].

3 Code Benchmarking

3.1 Free-flight calculations

To the best of our knowledge, no analytic theory or model describing the ion-drag to dust in magnetized plasmas has been published. In the "free-flight" regime however, where no electric field but the convective field driving the cross-field flow is considered, some analytic or semi-analytic calculations are possible. The free-flight model is of particular interest to the study of zero-Debye

[1] Eqs (21,24) are equivalent to Eqs (VII.42, VII.46) in Ref. [17], although expressed here in a simpler form.

length plasmas, because its solution (outside the infinitesimal Debye sheath) tends to the full problem solution in the limit of hot ions ($\tau \gg 1$), as discussed in Refs [12, 4].

In finite Debye length plasmas however, the conducting dust shields the convective electric field over a finite distance ($\sim \Lambda_{De}$) that cannot be disregarded. Because the convective electric potential in ion thermal units is independent of τ:

$$\chi_{\text{conv}} = -\frac{Ze}{T_{i\infty}} \left[E_{\text{conv}} R_p\right] = \sqrt{\pi} w_\perp \beta_i, \tag{25}$$

only when $w_\perp = 0$ does the free-flight solution correspond to the hot-ions limit. Its study is however useful as a way to gain physical insight as well as to benchmark the SCEPTIC3D code against independent solutions.

In the free-flight regime, at the dust surface only the ion collection force $\mathbf{F^p_{im}}$ is non-zero. In unmagnetized plasmas, it is straightforwardly given by integration of the moment of an unperturbed shifted Maxwellian over the sphere surface (or by letting $\chi_p \to 0$ in Eq. (10) from Ref. [2]):

$$\mathbf{F^p_{im}} = F_i^0 \left\{ \frac{\pi}{2} \left[4w_d^2 + 4 - \frac{1}{w_d^2} \right] \text{erf}\left(w_d\right) + \frac{\sqrt{\pi}}{w_d} \left(2w_d^2 + 1\right) \exp\left(-w_d^2\right) \right\} \mathbf{e_d}. \tag{26}$$

The collection force can be computed semi-analytically in the entire range of ion magnetization $\beta_i \in [0, \infty]$ only when the flow is purely parallel. The solution is discussed in chapter VII, section 2.1 of Ref. [17]. In the presence of cross-field flow, it is possible to find semi-analytic expressions for the free-flight force when $\beta_i = \infty$. The derivation being quite technical without significantly contributing to physical insight, we report it as appendix A.

Figure (2) shows the ion collection force $\mathbf{F^p_{im}}$ computed by direct orbit integration with SCEPTIC3D in free-flight conditions, in the presence of cross-field flow (velocity $w_d = 0.5$ and different drift to magnetic field angles δ). Excellent agreement is found with the analytic limits at $\beta_i = 0$ (Eq. (26)), and the connection to $\beta_i = \infty$ (Eqs (41,55,56)) is very smooth. This is an important benchmark of the ion orbit integrator implemented in SCEPTIC3D [15], in particular of its ability to accurately resolve the magnetized orbit-dust intersection.

Figure (2a) shows the force along the magnetic axis, where at $\delta = \pi/2$ it is zero by symmetry; Fig. (2b) shows the force in the cross-field direction, and Fig. (2c) in the flow direction. We notice that the force in the drift direction is almost not sensitive to δ, and almost no magnetic field effect is felt at $\beta_i \lesssim 1$. Also of interest is Fig. (2d), showing the impact force in (minus) the convective field direction, which for obvious symmetry reasons is zero at $\beta_i = 0$. As magnetization increases, the ions, whose gyrocenter motion is in the $\mathbf{e_y}$ direction, strike the dust preferentially at $y < 0$ with a phase such that the velocity in the $\mathbf{e_x}$ direction is positive. The force seems to peak at $\beta_i \sim 0.8$, but does not tend to zero when $\beta_i \to \infty$. Indeed the Lorentz force experienced by the ions during their last Larmor gyration before collection is proportional to the magnetic field, while the Larmor radius is inversely proportional to that field: the Lorentz force work tends to a constant at high field.

3.2 Momentum conservation

In self-consistent steady-state operation, the ion-drag force to the dust particle must be equal to the *total* net flux of momentum to the computational domain, minus the external forces on the dust particle. It is therefore sum of

(a) Along $\mathbf{e_z}$ (i.e. $\parallel$ to $\mathbf{B}$)

(b) Along $\mathbf{e_y}$ (i.e $\perp$ to $\mathbf{B}$ and $\mathbf{E}_{\rm conv}$)

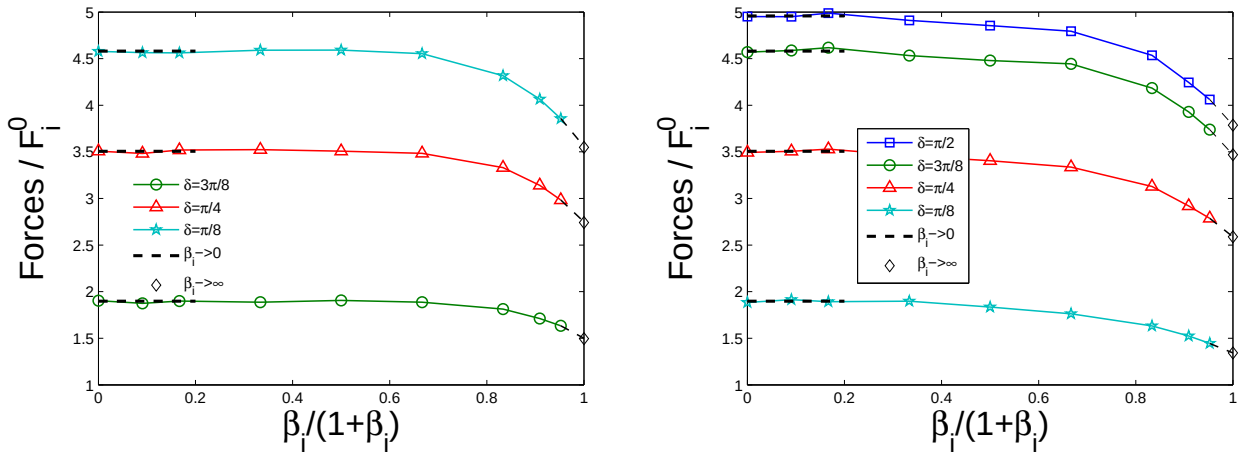

(c) Along $\mathbf{w_d}$

(d) Along $\mathbf{e_x}$ (i.e. $\parallel$ to $-\mathbf{E}_{\rm conv}$)

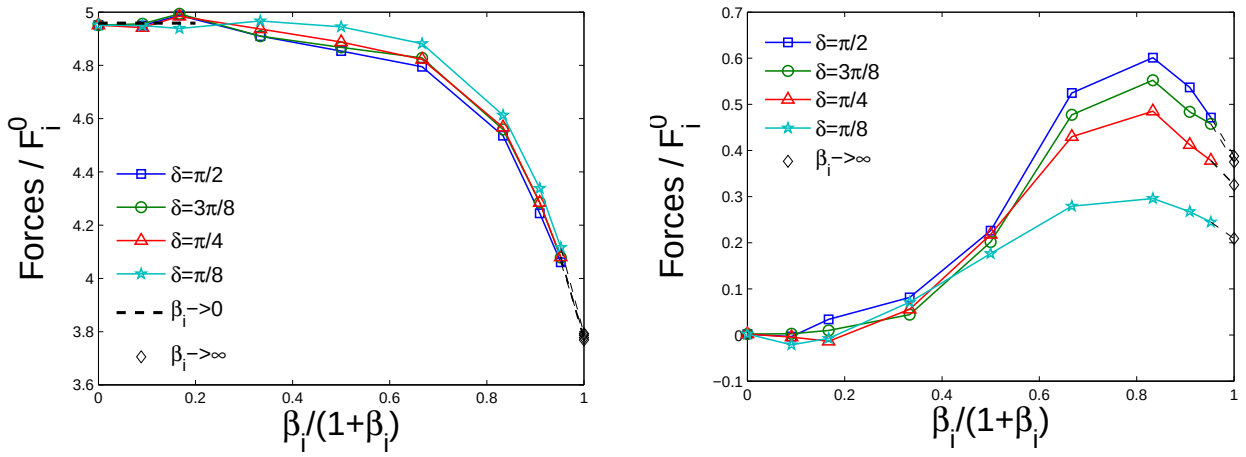

Figure 2: Ion-drag normalized to $F_i^0 = N_\infty R_p^2 T_{i\infty}/Z$ as a function of ion magnetization β_i in the free-flight regime (i.e. disregarding dust-induced electric field effects on the ions), computed by SCEPTIC3D for $w_d = 0.5$ and different drift to magnetic field angles δ along different axis. (a) Along the magnetic axis, (b) along the cross-field axis, (c) along the drift axis (i.e. weighted sum of (a) and (b)), and (d) along the convective electric field axis. The thick dashed lines indicate the analytic unmagnetized limit (Eq. (26)), and the dashed lines connect the last SCEPTIC3D point to the strongly magnetized limit (diamonds) given by Eqs (41,55,56).

- the electrostatic Maxwell stress integrated over the computational domain boundary ($\mathbf{F^o_E}$), only computed from the dust-induced potential perturbation Φ,
- the ion momentum flux $\mathbf{F^o_{im}}$,
- the electron pressure $\mathbf{F^o_e}$, non negligible at the outer boundary where the potential is small but not necessarily zero (see Ref. [5] for more details on the outer boundary conditions),
- the magnetostatic Maxwell stress integrated over the computational domain boundary minus the dust surface, which by analogy with Eq. (14) is the integral over the entire computational domain of the Lorentz force acting on the ions. From this must be subtracted the volumetric momentum flux due to the convective electric field acting on the ions, resulting in a total "Magnetic" contribution

$$\mathbf{F^o_M} = e \int_{\text{Domain}} (\langle \mathbf{v} \rangle - \mathbf{v_d})\, \mathrm{d}\Omega \times \mathbf{B}, \tag{27}$$

  where $\langle \mathbf{v} \rangle$ is the ion fluid velocity. As mentioned in section 2.1, the cross-field velocity of thermal electrons is everywhere equal to the *background* "$\mathbf{E} \times \mathbf{B}$" velocity, therefore $(\langle \mathbf{v_e} \rangle - \mathbf{v_d}) \times \mathbf{B} = 0$ in the entire simulation volume and $\mathbf{F^o_M}$ has no contribution from the electrons.

Figure (3) shows the ion-drag force evolution with increasing magnetic field self-consistently calculated with SCEPTIC3D in the presence of parallel and cross-field flow ($\delta = \pi/4$), along the three coordinate axes as well as projected on the drift direction $\mathbf{e_d}$ using the parameters $\lambda_{De} = 1$, $\tau = 0.1$, $v_d = 0.35 c_{s0}$, $\delta = \pi/4$ and $\phi_p = -8$. The contributions to the ion-drag force at the collecting sphere (solid lines) and outer boundary (dashed lines) are different, but very convincingly add up to the same total. This is a useful code cross-check of momentum conservation.

In unmagnetized plasmas, $\mathbf{F^o_{im}}$ can physically be identified with the ion collection force calculated with the binary collision approach $\mathbf{F^\infty_{im}}$ (see the introduction). Because the outer potential and potential gradient are not exactly zero however, it is the sum $\mathbf{F^o_e} + \mathbf{F^o_E}$ that should be identified with $\mathbf{F^\infty_E}$. Changing the domain size or the outer boundary condition (provided of course they remain reasonable) will mostly change the $\mathbf{F^o_E}$ to $\mathbf{F^o_e}$ balance, but have little impact on their sum or $\mathbf{F^o_{im}}$.

In section 4, only force calculations evaluated at the dust surface will be discussed.

4 Self-consistent force calculations

4.1 Low Debye length solutions

It is convenient to discuss SCEPTIC3D's solutions from small to large Debye lengths, starting in this paragraph with $\lambda_{De} = 0.03$. Figure (4) shows the ion-drag force computed at the dust surface in the presence of an equithermal ($\tau = 1$), purely perpendicular flow ($\delta = \pi/2$), for a drift velocity $v_d = 0.35 c_{s0}$. The dust potential is arbitrarily set to $\phi_p = -8$, and the ion magnetization allowed to vary from 0 to the maximum value such that no part of the dust particle is positively charged. The highest magnetizations considered here are $\beta_i = 10$ for $v_d = 0.35 c_{s0}$, corresponding to $\phi_{\text{conv}} \simeq -4.4$.

The first result is that the ion impact force along the $\mathbf{e_y}$-axis (i.e. the drift axis) is only weakly dependent on the magnetic field, as observed in the free-flight regime (section 3.1). The reason

(a) $\mathbf{e_y}$-axis

(b) $\mathbf{e_z}$-axis

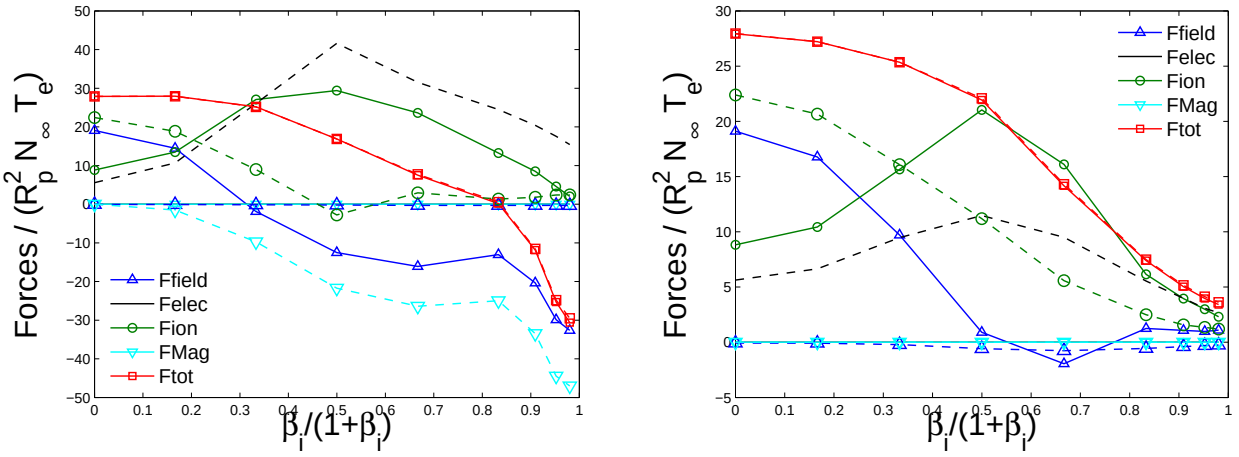

(c) $\mathbf{e_d}$-axis

(d) $\mathbf{e_x}$-axis

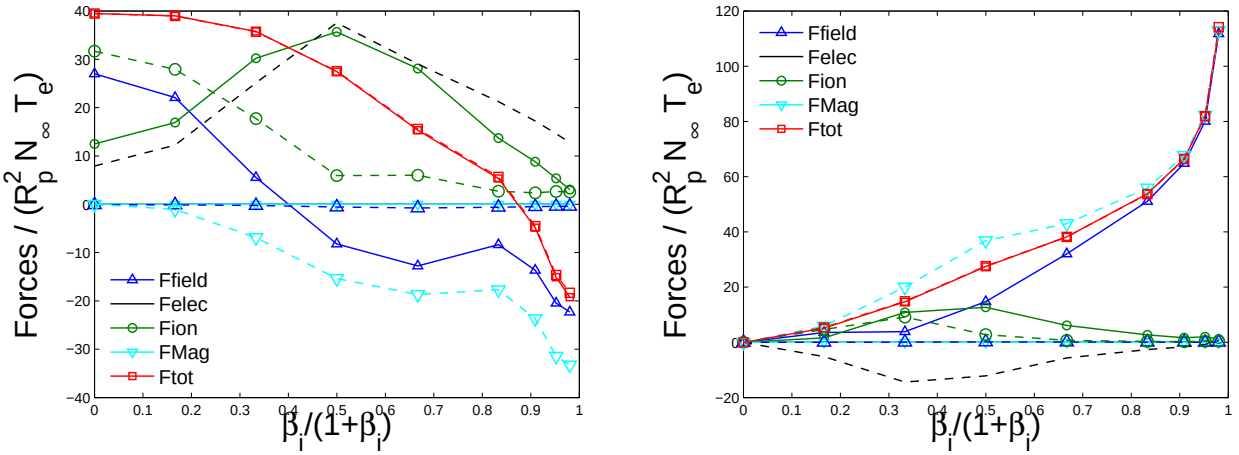

Figure 3: Example of SCEPTIC3D magnetized calculations for $\lambda_{De} = 1$, $\tau = 0.1$, $v_d = 0.35 c_{s0}$, $\delta = \pi/4$, $\phi_p = -8$, and increasing ion magnetization β_i on a computational domain of radius $r_b = 8$. The contributions to the ion-drag force at the collecting sphere (solid lines) and outer boundary (dashed lines) are different, but add up to the same total. "Ffield" refers to the electrostatic Maxwell stress F_E, "Felec" to the electron pressure force F_e, "Fion" to the ion collection force F_{im}, "FMag" to the integral over the computational domain volume of the Lorentz force minus the convective force F_M, and "Ftot" to the total ion-drag force F_i.

here is that because $\Lambda_{De} \ll R_L$, changing R_L has little impact on the ion dynamics in the Debye sheath. More surprisingly we notice that the electrostatic part of the ion-drag along the same drift axis is negative. The explanation is that the dust "pulls" on the ions as they are attracted, and by reaction feels a negative electrostatic drag. This pull effect increases with β_i, as the ions start to behave as beads on a wire moving at the "$\mathbf{E} \times \mathbf{B}$" velocity ($v_\perp = v_d$ here). A similar phenomenon has been documented in unmagnetized, strongly collisional plasmas [10, 18], where the dust pulls on upstream ions, who later "disappear" through charge exchange collisions.

At $\beta_i = 0$, momentum conservation implies that the *total* ion-drag be positive, which we observe here; no such requirement exists in the presence of a magnetic field since the external electric field is allowed to work on the ions, but it appears that regardless of β_i the ion-drag in the flow direction remains positive.

The ion impact force along the $\mathbf{e_x}$-axis is positive, and does not tend to zero at infinite magnetization as demonstrated in the free-flight regime (section 3.1). The electrostatic part of the ion-drag along the $\mathbf{e_x}$-axis is positive and increases with ion magnetization. This force arises from the plasma polarization induced by the dust effective dipole feeding back on the dust monopole; a crude estimate of its magnitude is given by the linearized solution (31), stating that $\mathbf{F^p_{E}}_x$ should be approximately proportional to β_i and $v_\perp$, which can easily be verified in Fig (4b).

(a) $\mathbf{e_y}$-axis (b) $\mathbf{e_x}$-axis

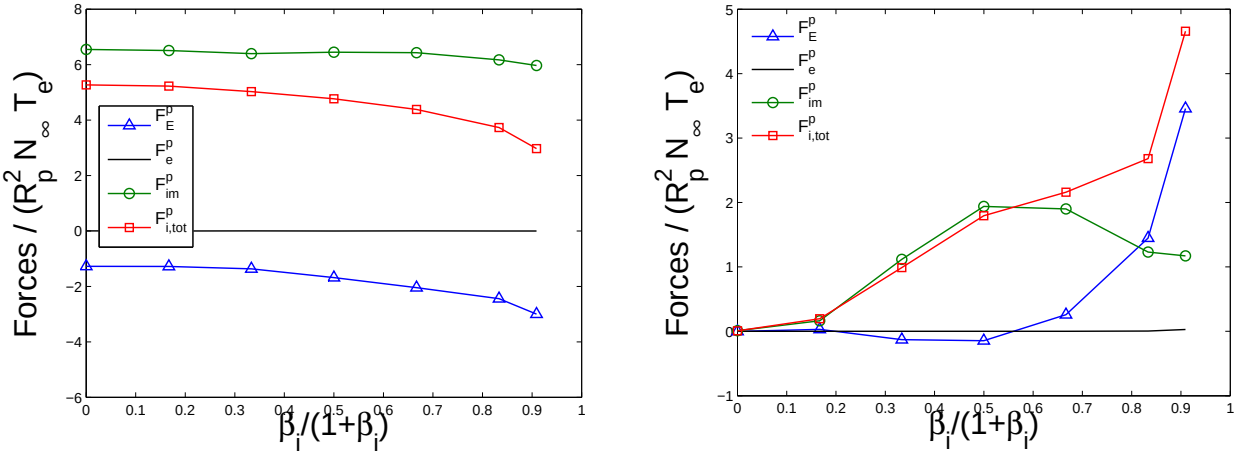

Figure 4: Ion-drag force components computed at the inner boundary (dust surface) by SCEPTIC3D for increasing ion magnetization β_i using the parameters $\tau = 1$, $\lambda_{De} = 0.03$, $\phi_p = -8$, and $v_d = 0.35 c_{s0}$. The flow is purely transverse ($\delta = \pi/2$), hence forces along the magnetic axis $\mathbf{e_z}$ are zero by symmetry.

Figure (5) shows that the $\mathbf{e_y}$ component of the internal Lorentz, as given by Eq. (24), becomes stronger than the ion-drag when $\beta_i \sim 2$. The positive sign of $\mathbf{F^p_j}_x$ is due to the electrons being predominantly collected at $x < 0$ (weakly electron-repelling zone), while the ion collection pattern is more isotropic or shifted towards $x > 0$ (strongly ion-attracting zone). This results in the internal dust current flowing predominantly in the $-\mathbf{e_x}$ direction. For the same reason $|\mathbf{F^p_j}_y| > |\mathbf{F^p_j}_x|$.

Perhaps the most surprising result of Fig. (5) is that the magnitude of $\mathbf{F^p_j}_x$ and $\mathbf{F^p_Q}$ are compa-

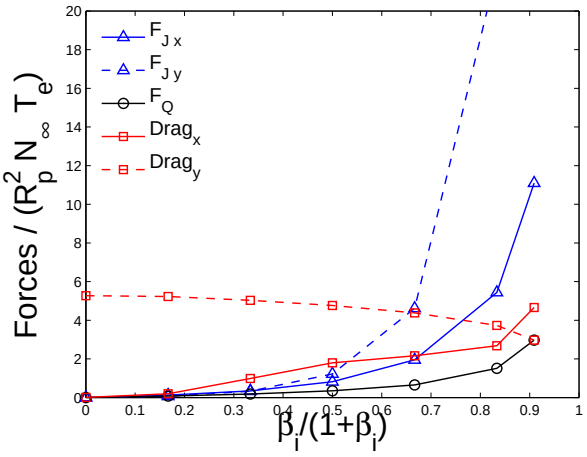

Figure 5: Comparison of the total ion-drag force computed by SCEPTIC3D with the parameters of Fig. (4), with the external forces $\mathbf{F_j^p}$ (computed from Eqs (21,24)) and $\mathbf{F_Q^p}$. For easy reading, lines referring to forces acting along $\mathbf{e_x}$ are solid, and dashed for $\mathbf{e_y}$.

rable to the drag, $\mathbf{F_{i}}_x$. In our treatment where the dust is stationary and the plasma flowing, $\mathbf{F_Q^p}$ arises from the convective field action on the dust charge. In most situations however, the dust is moving in a stationary plasma, and a straightforward Lorentz transform shows that in that case $\mathbf{F_Q^p}$ corresponds to the "$\mathbf{v} \times \mathbf{B}$" force responsible for the dust Larmor rotation. In small Debye length plasmas, a dust particle's Larmor angular frequency is therefore significantly faster than what is predicted by the simple-minded formula QB/m_{Dust}.

4.2 Debye-Hückel interpretation of the transverse electrostatic contribution

We see in Fig. (4b) (and also in Fig. (3d), although more crowded) that the electrostatic part of the ion-drag $\mathbf{F_E^p}$ (computed at the particle surface) has a transverse component antiparallel to $\mathbf{E}_{\mathrm{conv}}$. Because this force can have a significant impact on dust dynamics, we here briefly discuss its physical origin.

In the frame moving at velocity $\mathbf{v}_\perp$, where the convective electric field vanishes, the dust surface carries a dipole moment in addition to its charge Q (see Eq. (7)). The dust particle can therefore be seen as a "monopole+dipole" system in a conducting cage of radius $\sim \Lambda_{De}$ (Λ_{De} is the characteristic distance over which the potential is shielded by the electrons), inducing a polarization on the cage feeding back on the monopole. This simple picture can be formalized by a two-dimensional Debye-Hückel calculation as follows.

We neglect the ion response (i.e. $ZN_i = N_\infty$ in the entire domain), and limit ourselves to situations where $\Lambda_{De} \gg R_p$, implying that the potential variation close to the dust is governed by the electron density at a distance where it is almost unperturbed. Poisson equation can therefore be linearized about space potential $\Phi_0 = 0$; in spherical coordinates:

$$\nabla^2\Phi = \frac{1}{R^2}\frac{\partial}{\partial R}\left(R^2\frac{\partial\Phi}{\partial R}\right) + \frac{1}{R^2\sin\theta}\frac{\partial}{\partial\theta}\left(\sin\theta\frac{\partial\Phi}{\partial\theta}\right) + \frac{1}{R^2\sin^2\theta}\frac{\partial^2\Phi}{\partial\psi^2} = \frac{\Phi}{\Lambda_{De}^2}. \qquad (28)$$

Equation (28) can be solved by separation of variables, upon defining $\Phi(R,\theta,\psi)=\Xi(R)Y_\theta(\theta)Y_\psi(\psi)$. The angular potential dependence is then given by the Legendre polynomials $Y_\theta(\theta)Y_\psi(\psi)=P_l^m(\theta,\psi)$, with l positive integer and $m\in[-l:l]$, and the radial dependence by the solution of

$$\frac{1}{\Xi}\frac{\partial}{\partial R}\left(R^2\frac{\partial \Xi}{\partial R}\right)-\frac{R}{\Lambda_{De}^2}=l(l+1). \tag{29}$$

The solution of Eq. (28) satisfying the inner boundary condition Eq. (7) and decaying at infinity is

$$\Phi=\left[\Phi_p\frac{R_p}{R}+\Phi_{\text{conv}}\left(\frac{R_p}{R}\right)^2\frac{R+\Lambda_{De}}{R_p+\Lambda_{De}}\sin\theta\cos\psi\right]\exp\left(-\frac{R-R_p}{\Lambda_{De}}\right), \tag{30}$$

showing that the perturbed electrostatic potential distribution has a dipole term in addition to the well-known Debye-Hückel potential $\Phi(R)\propto\exp\left[-\left(R-R_p\right)/\Lambda_{De}\right]/R$. The sphere-integrated electrostatic force (Eq. (9)) on the dust is then readily calculated as

$$\mathbf{F_E^p}=\frac{4}{3}\pi\epsilon_0\frac{R_p^2}{\Lambda_{De}^2}R_p\Phi_p\mathbf{E}_{\text{conv}}=F_e^0\frac{4}{3}\pi\phi_p\phi_{\text{conv}}\mathbf{e_x}. \tag{31}$$

Equation (31) states that $\mathbf{F_E^p}$ is proportional to $\mathbf{E}_{\text{conv}}$, hence to β_i, which is the qualitative trend observed in Figs (3d,4b) (notice that the abscissa is $\beta_i/\left(1+\beta_i\right)$). Of course the agreement is only qualitative since the Debye-Hückel treatment is linearized and neglects the ion response.

This force can be compared to the external force $\mathbf{F_Q^p}$ (Eq. (12). The Debye-Hückel sphere capacitance is $C=4\pi\epsilon_0\left(1+R_p/\Lambda_{De}\right)R_p$, yielding

$$\mathbf{F_Q^p}=4\pi\epsilon_0\left(1+\frac{R_p}{\Lambda_{De}}\right)R_p\Phi_p\mathbf{E}_{\text{conv}}=F_e^0 4\pi\lambda_{De}^2\left(1+\frac{1}{\lambda_{De}}\right)\phi_p\phi_{\text{conv}}\mathbf{e_x}. \tag{32}$$

For completeness we mention that Daugherty and coauthors [19] performed similar calculations in a very different context. They considered the electrostatic force on an isolated particulate in an unmagnetized low-pressure (i.e. collisional) discharge, in the presence of an ion drift induced by a parallel electric field whose role is to compensate ion-neutral friction. The final formal expression for the forces is the same: Equation (13) in Ref. [19] corresponds to $\mathbf{F_E^p}+\mathbf{F_Q^p}$ (Eqs (31,32) in our treatment).

4.3 Intermediate and large Debye length solutions

Figures (6,7) show a gallery of ion-drag force computations for $\lambda_{De}\in[0.3:20]$ and $v_d\in[0.2:1.5]c_{s0}$, the other parameters being set as in Fig. (4).

We start the analysis with the forces along $\mathbf{e_y}$ (drift direction, since $\delta=\pi/2$), in Fig (6). It can first be seen that in intermediate and large Debye length conditions, the ion impact force behaves as in the short Debye length regime, i.e. almost no magnetic field effect is felt when $\beta_i\lesssim 1$. A crude estimate of $\mathbf{F_{im}^p}$ at low magnetic field can be obtained by multiplying the ion mass current to the dust by the characteristic velocity at which the ions are collected, yielding $F_{im}^p\sim\left(mI_i/Z\right)\left(v_d^2+v_{ti}^2\chi_p\right)^{1/2}$. Therefore as the Debye length increases past $\lambda_{De}\sim 1$, when the ion current approaches the large Debye length limit (OML at $\beta_i=0$ for instance), the ion impact force is not affected by a further increase in λ_{De}. At low drift velocity, in particular when the Debye

length is large, we can distinguish a slight peak in ion collection force at intermediate magnetization, whose origin is similar to the ion current peak discussed in Ref. [5].

The physics of the electrostatic force $\mathbf{F_E^p}$ is more complex. At $\beta_i = 0$, it increases continuously with λ_{De}, from the negative values observed in Fig. (4) at low Debye length to highly positive values proportional to the Coulomb logarithm at large Debye length [3]. Therefore the relative weight of $\mathbf{F_{im}^p}$ and $\mathbf{F_E^p}$ inverts at intermediate Debye length. The most surprising result here is that at intermediate Debye length and low enough drift velocity, the *total* ion-drag can reverse. The dust pulls on the upstream ion flow, which contrary to the short Debye length regime discussed in section 4.1 is deflected by the dust and only collected with parallel momentum. Indeed as shown in Ref. [5], strongly magnetized ions can only be collected with a parallel gyrocenter motion because the convective electric field driving the cross-field flow is shielded in the vicinity of the conducting dust particle.

Figure (7) shows the ion-drag for the same runs as in Fig. (6), but along the $\mathbf{e_x}$-axis. An interesting point is that the electrostatic drag $\mathbf{F_E^p}$ reverses between $\lambda_{De} = 3$ and $\lambda_{De} = 20$, a phenomenon for which we have no concrete explanation.

We now need to compare the just-computed ion-drag with the additional forces felt by the dust particle. Figure (8) shows that, similarly to what is observed at $\lambda_{De} = 0.03$ in Fig. (5), the magnitude of the $\mathbf{e_y}$-component of the internal Lorentz force given by Eq. (24) becomes stronger than the ion-drag when $\beta_i \sim 2$. It therefore seems that although the cross-field ion-drag can reverse, the *total* force felt by the dust particle is very unlikely to do so. It is for this very reason that we concluded in Ref. [20] that although the ion-drag force can indeed reverse in unmagnetized strongly collisional plasmas, external forces are much larger in magnitude so that no spontaneous dust motion should occur. Because SCEPTIC3D is not run in floating potential however, Eq. (24) is not exact and unlike Ref. [20] no definitive answer can be given here.

Analysis in the $\mathbf{e_x}$ direction is much easier, because as the Debye length increases the external electrostatic force $\mathbf{F_Q^p}$ becomes strongly dominant. Indeed $\mathbf{F_Q^p} = Q\mathbf{E}_{\text{conv}}$, and the dust charge Q is almost independent on the plasma Debye length when it is large enough (the capacitance tends to $C = 4\pi\epsilon_0 R_p$). All the other forces on the contrary are directly dependent on the ion current or the feedback of plasma polarization on the dust charge, both linearly depending on the plasma density N_∞, hence $\propto 1/\Lambda_{De}^2$ in absolute value. The reversal of $\mathbf{F_E^p}$ between $\lambda_{De} = 3$ and $\lambda_{De} = 20$ will therefore have no impact in practice.

5 Summary and conclusions

We report in this publication fully self-consistent calculations of the ion-drag force on a conducting spherical dust particle, when the background plasma has an $\mathbf{E} \times \mathbf{B}$-driven transverse flow (or equivalently the dust particle drifts across the magnetic force lines). Computations are performed with the hybrid PIC code SCEPTIC3D, whose capabilities have already been exploited in Refs [4, 5] to study ion collection.

The ion-drag force is computed by summing two terms: (a) the rate of ion momentum collection $\mathbf{F_{im}^p}$ (ion impact force), and (b) the electrostatic force on the negative dust charge arising from the flow-induced potential distribution anisotropy $\mathbf{F_E^p}$ (Eq. (13)). All other parameters unchanged and unless the Debye length is so large that other forces dominate, the qualitative effect of increasing the magnetic field is to decrease the ion-drag $\mathbf{F_i}$ in the flow direction, and increase it in the $-\mathbf{E}_{\text{conv}}$ direction. $\mathbf{F_{im}^p}$ always has a positive component in the flow direction, which is intuitive, but also

(a) $v_d = 0.2c_{s0}$, $\lambda_{De} = 0.3$ (b) $v_d = 0.2c_{s0}$, $\lambda_{De} = 3$ (c) $v_d = 0.2c_{s0}$, $\lambda_{De} = 20$

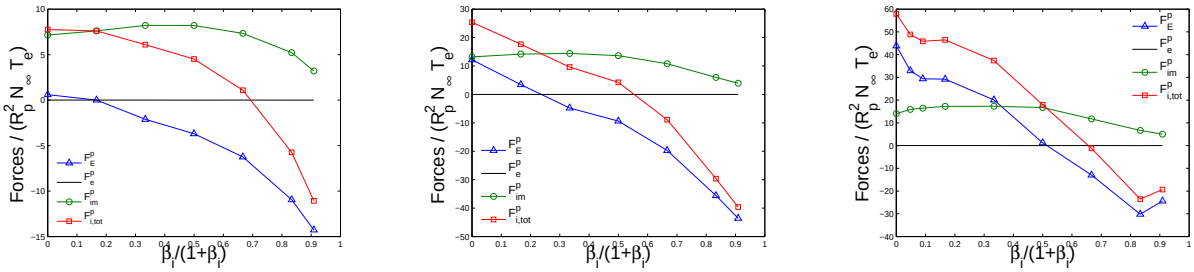

(d) $v_d = 0.5c_{s0}$, $\lambda_{De} = 0.3$ (e) $v_d = 0.5c_{s0}$, $\lambda_{De} = 3$ (f) $v_d = 0.5c_{s0}$, $\lambda_{De} = 20$

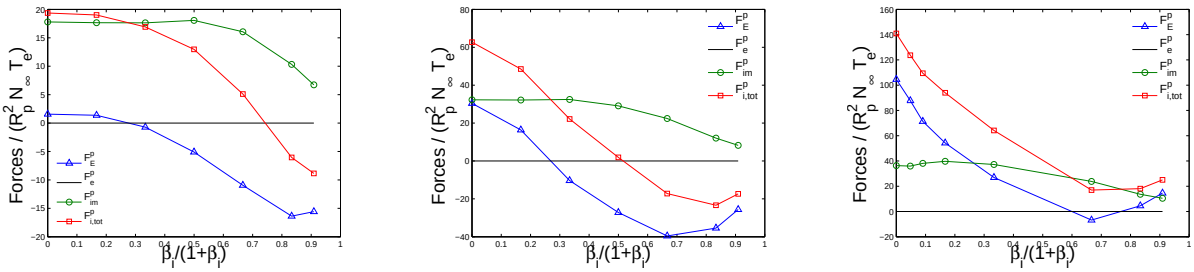

(g) $v_d = c_{s0}$, $\lambda_{De} = 0.3$ (h) $v_d = c_{s0}$, $\lambda_{De} = 3$ (i) $v_d = c_{s0}$, $\lambda_{De} = 20$

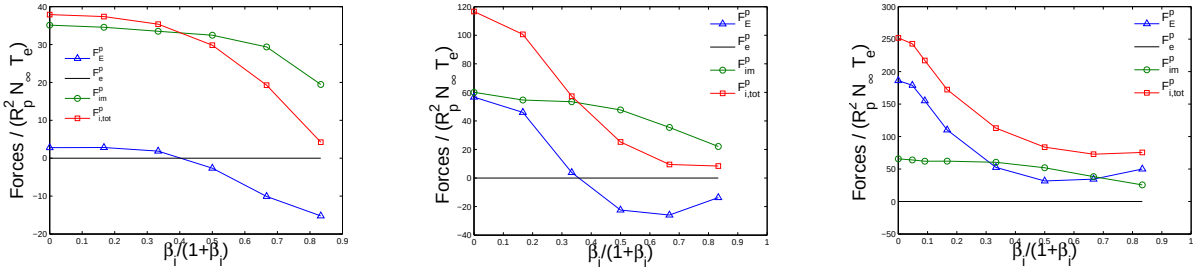

(j) $v_d = 1.5c_{s0}$, $\lambda_{De} = 0.3$ (k) $v_d = 1.5c_{s0}$, $\lambda_{De} = 3$ (l) $v_d = 1.5c_{s0}$, $\lambda_{De} = 20$

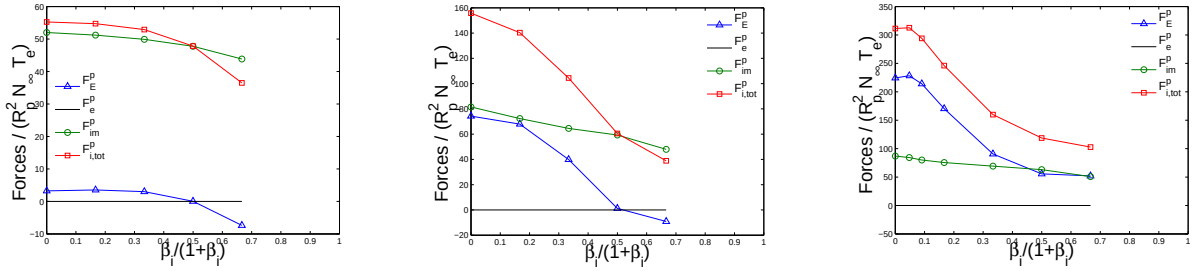

Figure 6: Ion-drag components computed at the dust surface by SCEPTIC3D along $\mathbf{e_y}$ as a function of β_i with $\tau = 1$, $\phi_p = -8$, $\delta = \pi/2$, and variable λ_{De} and v_d.

(a) $v_d = 0.2c_{s0}$, $\lambda_{De} = 0.3$ (b) $v_d = 0.2c_{s0}$, $\lambda_{De} = 3$ (c) $v_d = 0.2c_{s0}$, $\lambda_{De} = 20$

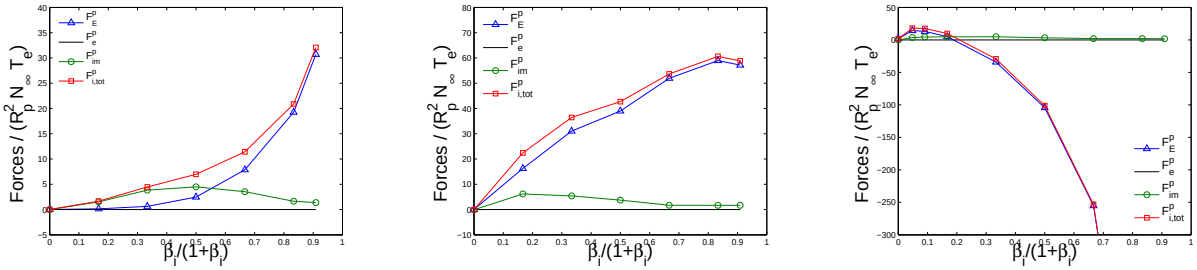

(d) $v_d = 0.5c_{s0}$, $\lambda_{De} = 0.3$ (e) $v_d = 0.5c_{s0}$, $\lambda_{De} = 3$ (f) $v_d = 0.5c_{s0}$, $\lambda_{De} = 20$

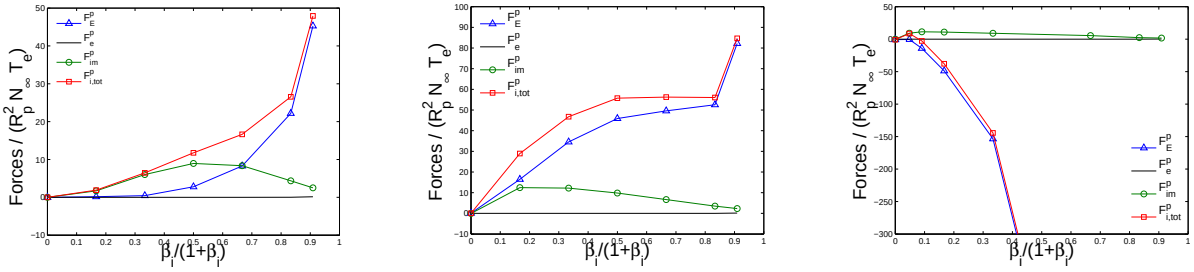

(g) $v_d = c_{s0}$, $\lambda_{De} = 0.3$ (h) $v_d = c_{s0}$, $\lambda_{De} = 3$ (i) $v_d = c_{s0}$, $\lambda_{De} = 20$

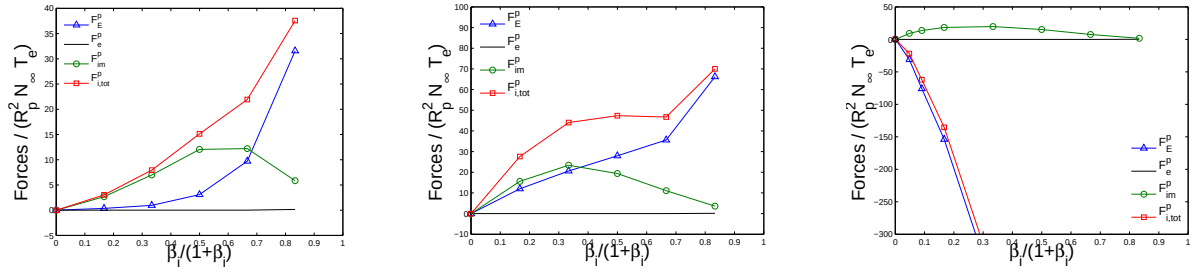

(j) $v_d = 1.5c_{s0}$, $\lambda_{De} = 0.3$ (k) $v_d = 1.5c_{s0}$, $\lambda_{De} = 3$ (l) $v_d = 1.5c_{s0}$, $\lambda_{De} = 20$

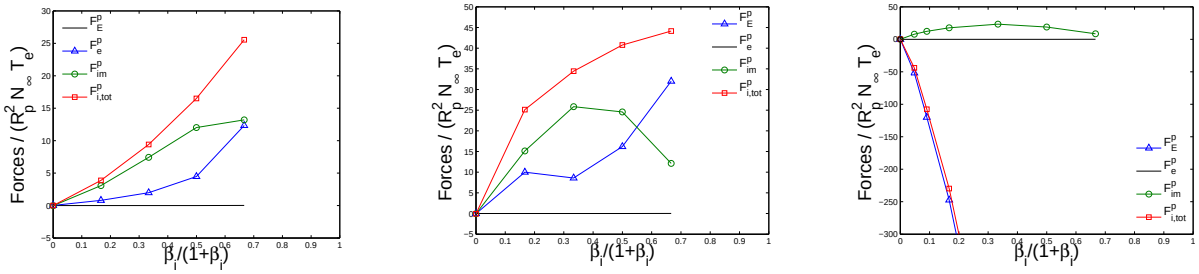

Figure 7: Ion-drag components along the convective field axis $\mathbf{e_x}$ computed at the inner boundary using the parameters of Fig. (6).

(a) $v_d = 0.2c_{s0}$, $\lambda_{De} = 0.3$ (b) $v_d = 0.2c_{s0}$, $\lambda_{De} = 3$ (c) $v_d = 0.2c_{s0}$, $\lambda_{De} = 20$

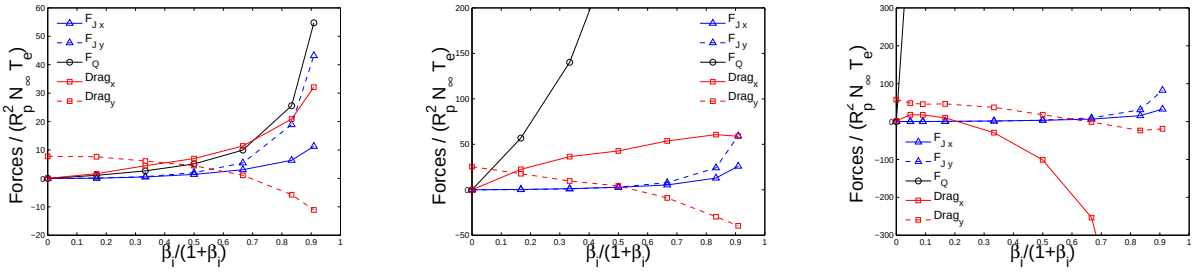

(d) $v_d = 0.5c_{s0}$, $\lambda_{De} = 0.3$ (e) $v_d = 0.5c_{s0}$, $\lambda_{De} = 3$ (f) $v_d = 0.5c_{s0}$, $\lambda_{De} = 20$

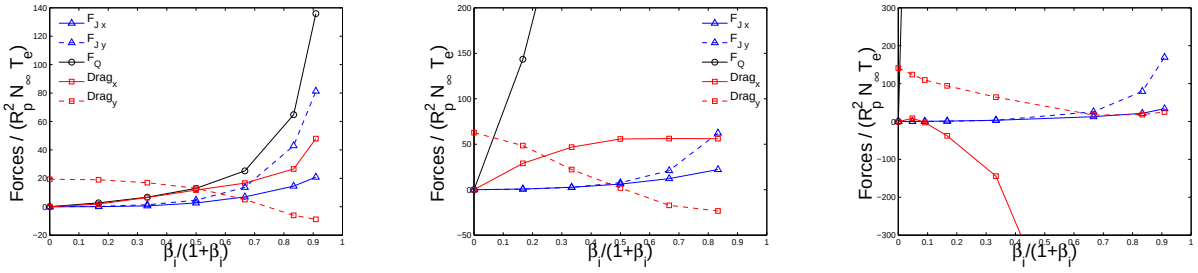

(g) $v_d = c_{s0}$, $\lambda_{De} = 0.3$ (h) $v_d = c_{s0}$, $\lambda_{De} = 3$ (i) $v_d = c_{s0}$, $\lambda_{De} = 20$

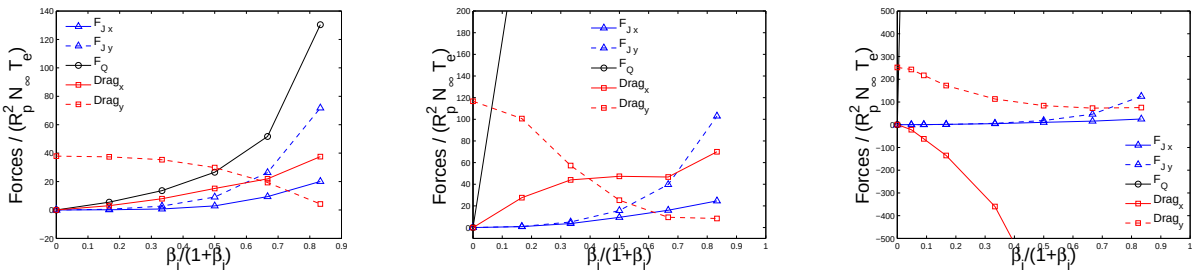

(j) $v_d = 1.5c_{s0}$, $\lambda_{De} = 0.3$ (k) $v_d = 1.5c_{s0}$, $\lambda_{De} = 3$ (l) $v_d = 1.5c_{s0}$, $\lambda_{De} = 20$

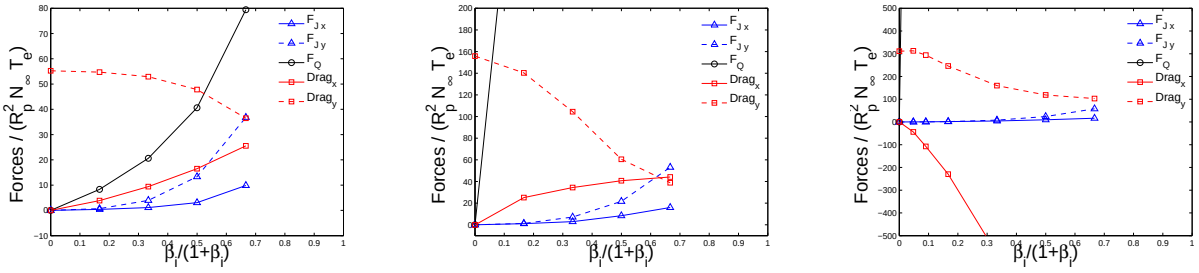

Figure 8: Comparison of the total ion-drag force computed by SCEPTIC3D with the parameters of Fig. (6), with the external forces $\mathbf{F_j^p}$ (Eqs (21,24)) and $\mathbf{F_Q^p}$. For easy reading, lines referring to forces acting along $\mathbf{e_x}$ are solid, and dashed for $\mathbf{e_y}$.

along $-\mathbf{E}_{\rm conv}$ due to asymmetries in the Lorentz force acting on the ions during their last Larmor rotation before collection. When the Debye length is short to intermediate however, we observe a reversal in $\mathbf{F}^{\mathbf{P}}_{\mathbf{E}}$ along the flow direction, strong enough for the total ion-drag in the flow direction to reverse. Approximate calculations of the net current circulating in the sphere (whose role is to balance asymmetries in ion and electron collection) however indicate that the internal Lorentz force should be in the positive direction and larger in magnitude than the ion-drag.

Also of interest to the study of dust dynamics is the observation that for short electron Debye lengths ($\Lambda_{De} \lesssim R_p$), the ion-drag and internal Lorentz force in the direction antiparallel to the convective electric field are in the same direction and have the same magnitude as $Q\mathbf{E}_{\rm conv}$. We therefore anticipate that in such conditions, dust particles should have a significantly faster gyromotion than what predicted by the Larmor formula QB/m_{Dust}.

Acknowledgments

Leonardo Patacchini was supported in part by NSF/DOE Grant No. DE-FG02-06ER54891. Most SCEPTIC3D calculations were performed on the MIT PSFC Parallel Opteron/Infiniband cluster Loki.

A Ion collection force at strong magnetization in the free-flight regime

A.1 Momentum flux to the magnetic presheath

In the plasma region, i.e outside the magnetic presheath, the ion motion at infinite magnetization can be treated in the drift approximation. In the frame moving at $v_\perp$ with respect to the dust particle (where the convective electric field is zero), the normalized ion distribution function splits into a "Larmor" part $f_L(w_L)$ describing the motion around the field lines, and a parallel part $f(w)$ describing the parallel motion. f_L is uniform in space because the magnetic momentum of strongly magnetized ions is conserved, and can easily be obtained from a 2D isotropic Maxwellian:

$$f_L(w_L) = 2w_L \exp\left(-w_L^2\right), \ w_L \in [0, \infty]. \tag{33}$$

f on the contrary must account for orbits depleted because directed away from the dust. In a free-flight treatment when $z > 0$:

$$f(w) = \frac{1}{\sqrt{\pi}} \exp\left[-\left(w - w_\infty\right)^2\right], \ w \in [-\infty, w_\perp \cot\eta], \tag{34}$$

where η is the angle of dust tangent to the magnetic field in a plane of transverse drift and magnetic field (See Fig. (9)). (x, η) define a parameterization of the dust surface, transformed from (θ, ψ).

The normalized ion charge-density n_i, parallel fluid velocity $\langle w \rangle$ and parallel temperature T_z can be computed from f's momenta. Using the notation $\mu_{ti} = w_\perp \cot\eta - w_\infty$ (see Ref. [12] for

(a) (b)

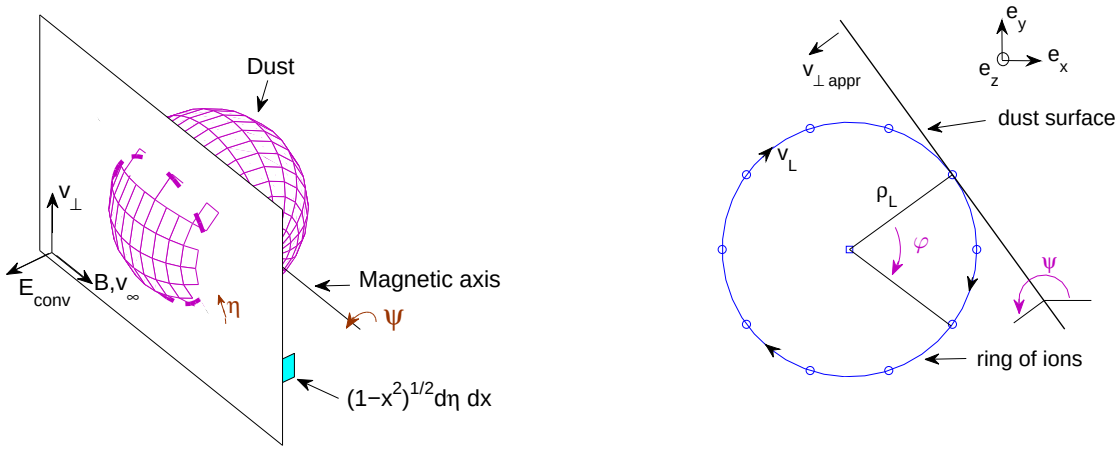

Figure 9: (a) Alternative "$x-\eta$" coordinate system (modified from Ref. [4]) and (b) dust surface approaching an ion ring with infinitesimal Larmor radius ρ_L with apparent velocity $v_{\perp\mathrm{appr}}$.

details):

$$n_i = \frac{1}{2}\mathrm{erfc}\left(-\mu_{ti}\right), \tag{35}$$

$$\langle w\rangle = w_\infty - \frac{1}{2n_i\sqrt{\pi}}\exp\left(-\mu_{ti}^2\right), \tag{36}$$

$$\frac{T_i}{T_{i\infty}} = 1 - \frac{2\mu_{ti}\sqrt{\pi}\exp\left(-\mu_{ti}^2\right)\mathrm{erfc}\left(-\mu_{ti}\right) + 2\exp\left(-2\mu_{ti}^2\right)}{\pi\mathrm{erfc}\left(-\mu_{ti}\right)^2}. \tag{37}$$

The momentum flux to an elementary magnetic presheath section located at x and η (cyan cross section in Fig. (9a)) is then given by

$$\mathrm{d}F^{\mathrm{mp}}_{im,z|\mathrm{Do}} = F_i^0 n_i \sin\eta\left[2\langle w\rangle\left(w_\perp\cot\eta - \langle w\rangle\right) - \frac{T_{iz}}{T_{i\infty}}\right]\left(1-x^2\right)^{1/2}\mathrm{d}x\mathrm{d}\eta, \tag{38}$$

$$\mathrm{d}F^{\mathrm{mp}}_{im,y|\mathrm{Do}} = F_i^0 n_i \sin\eta\left[2w_\perp\left(w_\perp\cot\eta - \langle w\rangle\right)\right]\left(1-x^2\right)^{1/2}\mathrm{d}x\mathrm{d}\eta, \tag{39}$$

$$\mathrm{d}F^{\mathrm{mp}}_{im,x|\mathrm{Do}} = 0. \tag{40}$$

Here, the subscript "|Do" indicates that the formula is valid in the downfield region $z>0$. Extension to the upfield region $z<0$ ("|Up") is trivial upon replacing w_∞ by $-w_\infty$.

Equations (35, 36) can readily be used to calculate the ion current to the infinitesimally thin magnetic presheath, equal to the collected current by virtue of charge conservation; this was the approach to Mach-probe analysis in Ref. [12]. Unfortunately transverse momentum is not conserved in the magnetic presheath, regardless of how thin it is, because of asymmetries in the Lorentz force acting on orbits intersecting the sphere. Therefore, while the total parallel force to the dust particle

is given by integration over x and η of Eq. (38) (the latter must be performed numerically):

$$F^p_{im,z} = \frac{\pi}{2}\left[\int_0^\pi \mathrm{d}F^{mp}_{im,z|\mathrm{Do}}\mathrm{d}\eta + \int_0^\pi \mathrm{d}F^{mp}_{im,z|\mathrm{Up}}\mathrm{d}\eta\right], \tag{41}$$

the transverse force equals the momentum flux from the plasma to the magnetic presheath

$$F^{\mathrm{mp}}_{im,y} = \frac{\pi}{2}\left[\int_0^\pi \mathrm{d}F^{mp}_{im,y|\mathrm{Do}}\mathrm{d}\eta + \int_0^\pi \mathrm{d}F^{mp}_{im,y|\mathrm{Up}}\mathrm{d}\eta\right], \tag{42}$$

corrected by the transverse ion momentum variation inside the magnetic presheath.

A.2 Force calculation

Our approach to calculating this correction is to first consider a ring of strongly magnetized ions with radius ρ_L (not necessarily equal to R_L, the average ion Larmor radius at infinity) gyrating with Larmor angular frequency Ω_L. The ions are uniformly spaced in pitch angle φ and at time $t = 0$ the ion at $\varphi = 0$ is in contact with a transverse plane moving towards the ring at velocity $w_{\perp\mathrm{appr}}$. An ion from the ring with initial pitch angle $\varphi_0 = \varphi\,(t = 0)$ will be collected by the plane at time t solution (or first positive solution if many) of

$$\rho_L \cos\left(\varphi_0 + \Omega_L t\right) = \rho_L - v_{\perp\mathrm{appr}} t. \tag{43}$$

Equation (43) is best treated in dimensionless form with $\sigma = \Omega_L t$ and

$$\alpha = \frac{w_{\perp\mathrm{appr}}}{w_L}, \tag{44}$$

yielding

$$\cos\left(\varphi_0 + \sigma\right) = 1 - \alpha\sigma. \tag{45}$$

Equation (45) can be solved for σ as a function of α and φ_0 by the Newton+bisection method, allowing to pretabulate the average change in ion pitch angle cosine and sine in the magnetic presheath for $\alpha \in [0 : \infty]$:

$$C(\alpha) = \frac{1}{2\pi}\int_0^{2\pi} \left[\cos\left(\varphi_0 + \sigma\left(\alpha, \varphi_0\right)\right) - \cos\varphi_0\right]\mathrm{d}\varphi_0, \tag{46}$$

$$S(\alpha) = \frac{1}{2\pi}\int_0^{2\pi} \left[\sin\left(\varphi_0 + \sigma\left(\alpha, \varphi_0\right)\right) - \sin\varphi_0\right]\mathrm{d}\varphi_0. \tag{47}$$

We now consider a ring of ions whose gyrocenter coordinate is $(x, y, z)(t)$ and velocity is $w\mathbf{e_z} + w_\perp \mathbf{e_y}$, colliding with the dust at position x and η, i.e. at a poloïdal angle ψ such that

$$\sin\psi = -\cos\eta\left(\frac{1 - x^2}{\cos^2\eta + x^2\sin^2\eta}\right)^{1/2}, \tag{48}$$

$$\cos\psi = \frac{x}{\left(\cos^2\eta + x^2\sin^2\eta\right)^{1/2}}. \tag{49}$$

A sketch of the colliding ion ring is shown in Fig. (9b). When close enough, it sees the dust as a flat surface approaching with transverse velocity $v_{\perp\mathrm{appr}} = -\mathrm{d}/\mathrm{d}t\left[\rho - \left(1-z^2\right)^{1/2}\right]$, where we recall that $\rho = \left(x^2+y^2\right)^{1/2}$:

$$w_{\perp\mathrm{appr}} = -\left(w_\perp - w\tan\eta\right)\sin\psi. \tag{50}$$

α therefore does not only depend on the impact position x and η, but also on w, $w_\perp$ and w_L. Integration of C and S over w, weighted by the ion flux-density, yields

$$c(w_L, w_\perp, x, \eta) = \int_{-\infty}^{w_\perp\cot\eta} \sin\eta\left[f\left(w\right)\left(w_\perp\cot\eta - w\right)\right] C(\alpha)\mathrm{d}w, \tag{51}$$

$$s(w_L, w_\perp, x, \eta) = \int_{-\infty}^{w_\perp\cot\eta} \sin\eta\left[f\left(w\right)\left(w_\perp\cot\eta - w\right)\right] S(\alpha)\mathrm{d}w, \tag{52}$$

enabling calculation of the momentum variation per elementary magnetic presheath surface located at x and η:

$$\mathrm{d}\delta F^{\mathrm{mp}}_{im,y|\mathrm{Do}} = 2F_i^0\left[\int_0^\infty \left(c\cos\psi - s\sin\psi\right) w_L f_L(w_L)\mathrm{d}w_L\right]\left(1-x^2\right)^{1/2}\mathrm{d}\eta\mathrm{d}x, \tag{53}$$

$$\mathrm{d}\delta F^{\mathrm{mp}}_{im,x|\mathrm{Do}} = 2F_i^0\left[\int_0^\infty \left(s\cos\psi + c\sin\psi\right) w_L f_L(w_L)\mathrm{d}w_L\right]\left(1-x^2\right)^{1/2}\mathrm{d}\eta\mathrm{d}x. \tag{54}$$

The total forces along $\mathbf{e_y}$ and $\mathbf{e_x}$ can then be integrated numerically as

$$F^p_{im,y} = F^{\mathrm{mp}}_{im,y} - \int_{-1}^{1}\left[\int_0^\pi \mathrm{d}\delta F^{\mathrm{mp}}_{im,y|\mathrm{Do}}\mathrm{d}\eta + \int_0^\pi \mathrm{d}\delta F^{\mathrm{mp}}_{im,y|\mathrm{Up}}\mathrm{d}\eta\right]\mathrm{d}x, \tag{55}$$

$$F^p_{im,x} = \quad 0 \quad - \int_{-1}^{1}\left[\int_0^\pi \mathrm{d}\delta F^{\mathrm{mp}}_{im,x|\mathrm{Do}}\mathrm{d}\eta + \int_0^\pi \mathrm{d}\delta F^{\mathrm{mp}}_{im,x|\mathrm{Up}}\mathrm{d}\eta\right]\mathrm{d}x. \tag{56}$$

References

[1] V.E. Fortov, A.C. Ivlev, S.A. Khrapak *et al. Complex (dusty) plasmas: Current status, open issues, perspectives*, Physics reports **421**, 1-103 (2005).

[2] I.H. Hutchinson, *Ion collection by a sphere in a flowing plasma: 3. Floating potential and drag force*, Plasma Phys. Control. Fusion **47**, 71-87 (2005).

[3] I.H. Hutchinson, *Collisionless ion drag force on a spherical grain*, Plasma Phys. Control. Fusion **48**, 2 (2006).

[4] L. Patacchini and I.H. Hutchinson, *Spherical probes at ion saturation in* $\mathbf{E}\times\mathbf{B}$ *fields*, Plasma Phys. Control. Fusion **52**, 035005 (2010).

[5] L. Patacchini and I.H. Hutchinson, *Spherical conducting probes in finite Debye length plasmas and* $\mathbf{E}\times\mathbf{B}$ *fields*, Plasma Phys. Control. Fusion **53**, 025005 (2011).

[6] I.H. Hutchinson, *Principles of Plasma Diagnostics*, 2nd ed. (Cambridge University press, Cambridge, UK, 2002).

[7] S.A. Khrapak, A.V. Ivlev, G.E. Morfill, and H.M. Thomas, *Ion drag force in complex plasmas*, Phys. Rev. E, **66**, 046414 (2002).

[8] S.A. Khrapak, A.V. Ivlev, G.E. Morfill, S.K. Zhdanov, and H.M Thomas, *Scattering in the attractive Yukawa potential: Application to the ion-drag force in complex plasmas*, IEEE trans. plasma sci., **32**, 2 (2004).

[9] A.V. Ivlev, S.A. Khrapak, S.K. Zhdanov, G.E. Morfill, and G. Joyce, *Force on a Charged Test Particle in a Collisional Flowing Plasma*, Phys. Rev. Letters, **92** 205007 (2004).

[10] S.A. Khrapak, S.K. Zhdanov, A.V. Ivlev, and G.E. Morfill, *Drag force on an absorbing body in highly collisional plasmas*, J. Appl. Physics **101**, 033307 (2007).

[11] H.N. Nitta, N. Nambu, N. Salimullah, and P.K. Shukla, *Dynamical potential in a magnetized plasma*, Phys. Letters A, **308** 451-454 (2003).

[12] L. Patacchini and I.H. Hutchinson, *Kinetic solution to the Mach probe problem in transversely flowing strongly magnetized plasmas*, Phys. Rev. E **80**, 036403 (2009).

[13] R.W Hockney and J.W. Eastwood, *Computer simulation using particles*, Taylor and Francis (1989).

[14] C.K. Birdsall and A.B. Langdon, *Plasma Physics via computer simulation*, Institute of Physics, Series in Plasma Physics (1991).

[15] L. Patacchini and I.H. Hutchinson, *Explicit time-reversible orbit integration in Particle In Cell codes with static homogeneous magnetic field*, J. Comp. Phys. **228**, 2604-2615 (2009).

[16] L. Patacchini, I.H. Hutchinson and G. Lapenta, *Electron collection by a negatively charged sphere in a collisionless magnetoplasma*, Phys. Plasmas **14**, 062111 (2007).

[17] L. Patacchini *PhD Thesis: Collisionless ion collection by non-emitting spherical bodies in* $\mathbf{E} \times \mathbf{B}$ *fields* MIT, PSFC RR-09-13 (2009).

[18] S.A. Khrapak, B.A. Klumov and G.E. Morfill Phys. Plasmas **14**, (response) 074702 (2007).

[19] J.E. Daugherty, R.K. Porteous and D.B. Graves, *Electrostatic forces on small particles in low-pressure discharges*, J. Appl. Phys, 73-4 1617-1620 (1993).

[20] L. Patacchini and I.H. Hutchinson, *Fully Self-Consistent Ion-Drag-Force Calculations for Dust in Collisional Plasmas with an External Electric Field*, Phys. Rev. Lett. **101**, 025001 (2008).